Tamm plasmon polaritons in multilayered cylindrical structures

C. E. Little,[1] R. Anufriev,[2] I. Iorsh,[1] M. A. Kaliteevski,[3,4] R. A. Abram,[1,*] and S. Brand[1]
[1]*Department of Physics, Durham University, Durham, DH1 3LE, United Kingdom*
[2]*Institut des Nanotechnologies de Lyon (INL)-UMR5270-CNRS, Université de Lyon, INSA-Lyon, 7 Avenue Jean Capelle, 69621 Villeurbanne, France*
[3]*St Petersburg Academic University, 8/3 Khlopina, St Petersburg, Russia*
[4]*Ioffe Physicotechnical Institute, 26, Polytechnicheskaya, St Petersburg, Russia*
(Received 29 May 2012; published 14 December 2012)

It is shown that cylindrical Bragg reflector structures with either a metal core, a metal cladding, or both can support Tamm plasmon polaritons (TPPs) that can propagate axially along the interface between the metallic layer and the adjacent dielectric. A transfer matrix formalism for cylindrical multilayered structures is used in association with cavity phase matching considerations to design structures that support Tamm plasmon polaritons at specified frequencies, and to explore the field distributions and the dispersion relations of the excitations. The cylindrical TPPs can exist in both the TE and TM polarizations for the special cases of modes with either azimuthal isotropy or zero axial propagation constant and also as hybrid cylindrical modes when neither of those conditions applies. In the cases considered the TPPs have low effective masses and low group velocities. Also, when there is both metallic core and cladding, near degenerate modes localized at each metallic interface can couple to produce symmetric and antisymmetric combinations whose frequency difference is in the terahertz regime.

DOI: 10.1103/PhysRevB.86.235425 PACS number(s): 78.67.−n

I. INTRODUCTION

Tamm plasmon polaritons (TPPs) are a type of optical excitation that can occur at the interface between a metal and a dielectric Bragg mirror and were first proposed theoretically in 2007 by Kaliteevski *et al.*[1] following the work of Kavokin *et al.* on Tamm states at the interface between two periodic dielectric structures.[2] The existence of TPPs was subsequently demonstrated experimentally by Sasin *et al.*[3] As for conventional surface plasmon polaritons, the decay of the electromagnetic field in the metal is due to the negative dielectric constant. However, the decay in the Bragg mirror is not due to total internal reflection but to the photonic band gap arising from the dielectric layered structure. In contrast to the case of conventional surface plasmons, TPPs can exist in both the TE and TM polarizations because both the Bragg reflector and the metal layer are essentially mirrors forming a cavity to confine the light. It has also been predicted that optical Tamm states can exist above the bulk plasma frequency for structures fabricated with appropriate materials.[4,5]

Since the initial reports of TPPs there has been rapidly growing interest in their properties, and a number of applications have been reported. Particular attention has been devoted to phenomena associated with excitons. For example TPPs have been shown experimentally to exhibit strong coupling with quantum well excitons,[6] including in extremely compact structures with just five high refractive index contrast layers in the Bragg reflector.[7] Very recently, lasing in an optically-pumped hybrid GaAs/silver Tamm structure has been demonstrated.[8] It has also been shown[9] that confined Tamm plasmon modes can exist under metallic microdisks and can be used to control by over two orders of magnitude the rate of spontaneous optical emission from quantum dots in their proximity. In a related development, it has been predicted that a structure can be designed to exhibit strong coupling between TPPs and exciton polaritons when a metal film is deposited on one of the Bragg reflectors forming the quantum microcavity.[10] Furthermore it has been suggested that by patterning the metal film it would be possible to create a guiding channel for an exciton-polariton condensate, facilitating a method of producing polariton integrated circuits with potential for use in ultrafast information processing.[11]

Recently hybrid states of cavity photons and Tamm plasmons have been observed in an organic microcavity with an incorporated thin silver layer.[12] More generally, strong optical absorbers using TPPs at a thick metal/truncated photonic crystal interface have been proposed and demonstrated.[13] TPPs have also been proposed for use in switches,[14] and highly efficient, unidirectional transmission in an all-optical diode has been demonstrated using the interface states between a one-dimensional photonic crystal structure of SiO_2 and TiO_2 and a thick layer of silver.[15] TPPs have been shown to exist at an interface between a photonic crystal and a magnetophotonic crystal[16] or a magnetic metal,[17] and the enhancement of Faraday rotation and sharp transmission peaks have been suggested as useful characteristics for magnetotunable filters.

Hitherto the focus has been on planar structures but there could well be applications for TPPs in cylindrical waveguides in the wider field of plasmonics. In particular, the cylindrical geometry is promising for delivering TPPs with high resolution to specific points in space, including surfaces. Cylindrical geometries to support surface plasmon polaritons have already received some attention. Pfeiffer *et al.*[18] studied SPPs occurring on the outside of a solid metal cylinder, and Schröter and Dereux have studied SPPs in a thin cylindrical tube where they found that there are two surface plasmon branches corresponding to symmetric and antisymmetric plasma distributions between the inner and outer metal/dielectric interfaces.[19] Also the inclusion of a metal core, layer, or cladding in an optical fiber structure allows SPP and hybrid SPP waveguide modes to be included

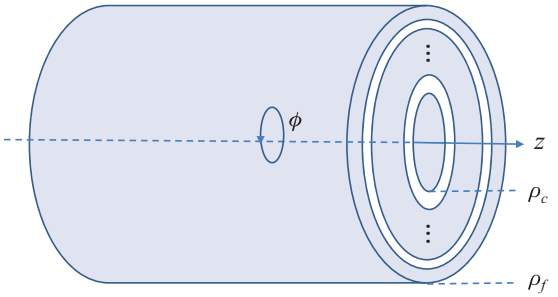

FIG. 1. (Color online) A cylindrical waveguide aligned along the z axis with a core region surrounded by layers of different refractive index. The dotted region represents repetition of the alternative refractive index layers. ρ_c and ρ_f indicate the radii of the core and the final layer of the structure respectively.

in the mode spectrum of the fiber. For example the dispersion of modes in optical fiber structures with a thin metal layer between the core and cladding was investigated in 1993 by Al-Bader and Imtaar[20] while a comprehensive study of step-index fibers where the core or cladding has negative dielectric constant was carried out in 1994 by Prade and Vinet.[21] More recently there has been interest in hybrid waveguides combining the advantages of well localized surface plasmon polaritons at metal dielectric interfaces and the long propagation lengths obtainable in traditional optical fiber-type structures.[22,23]

In this paper we consider the properties of TPPs in cylindrical Bragg reflector structures such as that illustrated in Fig. 1. The required metallic element can be included in the structure as either the core or as an outer cladding or placed in both locations. The transfer matrix method provides a rigorous and effective theoretical description of the TPP modes in such structures and is introduced in Sec. II A by describing the relevant formulas of that methodology in the cylindrical geometry. However, the design of structures that support modes with desirable properties[5] is greatly aided by consideration of the round trip phase change of a wave in the radial cavity formed by the Bragg reflector and the metal, and the details of that approach are presented in Sec. II B. The application of the theory and design methods to some example structures is described along with the results in Sec. III.

II. THEORY

A. Transfer matrix method

The modes of optical fibers and similar cylindrical structures can be obtained using the transfer matrix method described by Chew.[24] Consider modes at angular frequency ω with electric and magnetic fields of the form

$$\mathbf{E} = \mathbf{E}(\rho)\exp[i(\beta z + m\phi)]$$
$$\mathbf{B} = \mathbf{B}(\rho)\exp[i(\beta z + m\phi)]$$

in the cylindrical coordinates indicated in Fig. 1; β is the propagation constant and m is an integer or zero and describes the azimuthal variation of the fields.

The transfer matrix method in a circular cylindrical multilayered system facilitates the calculation of an electromagnetic field at a radius ρ given that the field at another radius, ρ_0, is already known. Specifically,

$$\begin{pmatrix} E_z(\rho) \\ cB_\phi(\rho) \\ cB_z(\rho) \\ E_\phi(\rho) \end{pmatrix} = \hat{M}(\rho_0,\rho) \begin{pmatrix} E_z(\rho_0) \\ cB_\phi(\rho_0) \\ cB_z(\rho_0) \\ E_\phi(\rho_0) \end{pmatrix}, \tag{1}$$

where $\hat{M}(\rho_0,\rho)$ is the 4×4 transfer matrix between the radii ρ_0 and ρ and we choose to represent the magnetic field in terms of $c\mathbf{B}$ so that all the vector components are expressed in the same units. The field components that make up the vectors in Eq. (1) are parallel to the interfaces in a multilayer waveguide. At the interface between two layers with different refractive indices these components must be continuous. The transfer matrix across a multilayer structure is the product of the transfer matrices for the individual layers correctly ordered to propagate the fields from the selected start point to the selected end point. Structures with a refractive index which varies continuously in the radial direction can be approximated by a multilayer structure with suitably thin layers. Once the vector on the left hand side of Eq. (1) has been determined, the radial field components may be calculated using Maxwell's curl equations.

The elements of $\hat{M}(\rho_0,\rho)$ for a homogeneous layer are:

$$\begin{aligned}
M_{11} &= k\rho_0\frac{\pi}{2}[N_m'(k\rho_0)J_m(k\rho) - J_m'(k\rho_0)N_m(k\rho)] \\
M_{21} &= in^2k_0\rho_0\frac{\pi}{2}[N_m'(k\rho_0)J_m'(k\rho) - J_m'(k\rho_0)N_m'(k\rho)] \\
&\quad + \frac{i\beta^2m^2}{k^2k_0\rho}\frac{\pi}{2}[N_m(k\rho_0)J_m(k\rho) - J_m(k\rho_0)N_m(k\rho)] \\
M_{31} &= -\frac{i\beta m}{k_0}\frac{\pi}{2}[N_m(k\rho_0)J_m(k\rho) - J_m(k\rho_0)N_m(k\rho)] \\
M_{41} &= -\frac{\beta m}{k}\frac{\rho_0}{\rho}\frac{\pi}{2}[N_m'(k\rho_0)J_m(k\rho) - J_m'(k\rho_0)N_m(k\rho)] \\
&\quad + \frac{\beta m}{k}\frac{\pi}{2}[N_m'(k\rho)J_m(k\rho_0) - J_m'(k\rho)N_m(k\rho_0)] \\
M_{12} &= \frac{ik^2\rho_0}{n^2k_0}\frac{\pi}{2}[N_m(k\rho_0)J_m(k\rho) - J_m(k\rho_0)N_m(k\rho)] \\
M_{22} &= k\rho_0\frac{\pi}{2}[N_m'(k\rho)J_m(k\rho_0) - J_m'(k\rho)N_m(k\rho_0)] \\
M_{32} &= 0 \\
M_{42} &= \frac{-i\beta m}{n^2k_0}\frac{\rho_0}{\rho}\frac{\pi}{2}[N_m(k\rho_0)J_m(k\rho) - J_m(k\rho_0)N_m(k\rho)] \\
M_{13} &= \frac{i\beta m}{n^2k_0}\frac{\pi}{2}[N_m(k\rho_0)J_m(k\rho) - J_m(k\rho_0)N_m(k\rho)] \\
M_{23} &= -\frac{\beta m}{k}\frac{\pi}{2}[N_m(k\rho_0)J_m'(k\rho) - J_m(k\rho_0)N_m'(k\rho)] \\
&\quad - \frac{\beta m}{k}\frac{\pi}{2}\frac{\rho_0}{\rho}[N_m'(k\rho_0)J_m(k\rho) - J_m'(k\rho_0)N_m(k\rho)] \\
M_{33} &= k\rho_0\frac{\pi}{2}[N_m'(k\rho_0)J_m(k\rho) - J_m'(k\rho_0)N_m(k\rho)] \\
M_{43} &= -\frac{i\beta^2m^2}{n^2k^2k_0\rho}\frac{\pi}{2}[N_m(k\rho_0)J_m(k\rho) - J_m(k\rho_0)N_m(k\rho)] \\
&\quad - ik_0\rho_0\frac{\pi}{2}[N_m'(k\rho_0)J_m'(k\rho) - J_m'(k\rho_0)N_m'(k\rho)]
\end{aligned} \tag{2}$$

$$M_{14} = 0$$
$$M_{24} = \frac{i\beta m}{k_0}\frac{\rho_0}{\rho}\frac{\pi}{2}[N_m(k\rho_0)J_m(k\rho) - J_m(k\rho_0)N_m(k\rho)]$$
$$M_{34} = -\frac{ik^2\rho_0}{k_0}\frac{\pi}{2}[N_m(k\rho_0)J_m(k\rho) - J_m(k\rho_0)N_m(k\rho)]$$
$$M_{44} = k\rho_0\frac{\pi}{2}[N_m^{'}(k\rho)J_m(k\rho_0) - J_m^{'}(k\rho)N_m(k\rho_0)],$$

where $J_m(x)$ and $N_m(x)$ are Bessel and Neumann functions respectively, $k^2 = n^2k_0^2 - \beta^2$, $k_0 = \omega/c$, and n is the refractive index of the medium.

The fields at the center of the cylindrical core, $\rho = 0$, must be finite and the radial dependence of their z components will have the form

$$E_z|_{\text{core}} = A_{1c}J_m(k_c\rho)$$
$$cB_z|_{\text{core}} = A_{2c}J_m(k_c\rho),$$

where A_{1c} and A_{2c} are constants and the subscript c denotes parameter values for the core region. Outside the waveguide at radius greater than $\rho = \rho_f$, if a decaying solution is possible and is sought, and we can write

$$E_z|_f = B_{1f}K_m(k_f\rho)$$
$$cB_z|_f = B_{2f}K_m(k_f\rho)$$

where $K_m(x)$ is a modified Bessel function of the second kind, B_{1f} and B_{2f} are constants and the subscript f denotes parameter values outside the final layer of the structure. Alternatively, for modes which leak from the waveguide the solution outside would be a propagating wave described by the Hankel function $H_m^{(1)}(x)$.

It follows that the fields at the inner edge of the core, ρ_c, can be written in matrix form as

$$\begin{pmatrix} E_z(k_c\rho_c) \\ cB_\phi(k_c\rho_c) \\ cB_z(k_c\rho_c) \\ E_\phi(k_c\rho_c) \end{pmatrix} = \begin{pmatrix} J_m(k_c\rho_c) & 0 \\ \frac{ik_0n_c^2}{k_c}J_m^{'}(k_c\rho_c) & -\frac{\beta m}{k_c^2\rho_c}J_m(k_c\rho_c) \\ 0 & J_m(k_c\rho_c) \\ -\frac{\beta m}{k_c^2\rho_c}J_m(k_c\rho_c) & -\frac{ik_0}{k_c}J_m^{'}(k_c\rho_c) \end{pmatrix}\begin{pmatrix} A_{1c} \\ A_{2c} \end{pmatrix}$$
$$= \hat{\Omega}_c\begin{pmatrix} A_{1c} \\ A_{2c} \end{pmatrix} \quad (3)$$

and those at the outside edge of the waveguide at radius ρ_f as

$$\begin{pmatrix} E_z(k_f\rho_f) \\ cB_\phi(k_f\rho_f) \\ cB_z(k_f\rho_f) \\ E_\phi(k_f\rho_f) \end{pmatrix} = \begin{pmatrix} K_m(k_f\rho_f) & 0 \\ \frac{ik_0n_f^2}{k_f}K_m^{'}(k_f\rho_f) & -\frac{\beta m}{k_f^2\rho_f}K_m(k_f\rho_f) \\ 0 & K_m(k_f\rho_f) \\ -\frac{\beta m}{k_f^2\rho_f}K_m(k_f\rho_f) & -\frac{ik_0}{k_f}K_m^{'}(k_f\rho_f) \end{pmatrix}$$
$$\times\begin{pmatrix} B_{1f} \\ B_{2f} \end{pmatrix} = \hat{\Omega}_f\begin{pmatrix} B_{1f} \\ B_{2f} \end{pmatrix}. \quad (4)$$

The fields at the outside edge of the waveguide may also be found by applying the appropriate transfer matrix $\hat{M}$ to the fields at the edge of the core. Using Eq. (1) with $\rho_0 = \rho_c$ and $\rho = \rho_f$ and Eqs. (3) and (4) for the fields at the edge of the core and the edge of the waveguide we have

$$\hat{M}\hat{\Omega}_c\begin{pmatrix} A_{1c} \\ A_{2c} \end{pmatrix} - \hat{\Omega}_f\begin{pmatrix} B_{1f} \\ B_{2f} \end{pmatrix} = \begin{pmatrix} 0 \\ 0 \end{pmatrix}$$
$$\left(\hat{M}\hat{\Omega}_c| - \hat{\Omega}_f\right)\begin{pmatrix} A_{1c} \\ A_{2c} \\ B_{1f} \\ B_{2f} \end{pmatrix} = \begin{pmatrix} 0 \\ 0 \\ 0 \\ 0 \end{pmatrix}, \quad (5)$$

where $(\hat{M}\hat{\Omega}_c| - \hat{\Omega}_f)$ is a 4×4 matrix where the first two columns are given by $\hat{M}\hat{\Omega}_c$ and the second two columns are given by $-\hat{\Omega}_f$. Equation (5) has nonzero solutions for A_{1c}, A_{2c}, B_{1f}, and B_{2f} when the determinant of $(\hat{M}\hat{\Omega}_c| - \hat{\Omega}_f)$ is equal to zero. Modes of a multilayer structure can be found numerically by initially specifying the physical parameters of the structure under consideration, allowing the frequency to vary and searching for the roots of the determinant. The coefficients A_{1c}, A_{2c}, B_{1f}, and B_{2f} can then be found for the given frequency by solving the simultaneous equations in Eq. (5).

For the special cases of either the azimuthal number, $m = 0$, or the propagation constant, $\beta = 0$, the problem is reduced to a more straightforward one involving 2×2 matrices. That is because the field components E_ρ, E_ϕ, cB_ρ, and cB_ϕ can each be expressed in terms of just E_z and cB_z using Maxwell's curl equations and although, in general, the formulas involve both E_z and cB_z, setting $m = 0$ or $\beta = 0$ results in a decoupling. For the case of $\beta = 0$, which corresponds to no propagation of the mode along the waveguide axis, there are two distinct types of mode: those with just the components E_ρ, E_ϕ, and cB_z (TE modes), or those with E_z, cB_ρ, and cB_ϕ (TM modes). Similarly for $m = 0$, there is a mode with components E_ϕ, cB_ρ, and cB_z (a TE mode), and a mode with components E_ρ, E_z, and cB_ϕ (a TM mode).

The 2×2 transfer matrices, $\hat{T}^{TE}$ for the TE modes are defined by

$$\begin{pmatrix} cB_z(\rho) \\ E_\phi(\rho) \end{pmatrix} = \hat{T}^{TE}\begin{pmatrix} cB_z(\rho_0) \\ E_\phi(\rho_0) \end{pmatrix}, \quad (6)$$

and for the TM modes by

$$\begin{pmatrix} E_z(\rho) \\ cB_\phi(\rho) \end{pmatrix} = \hat{T}^{TM}\begin{pmatrix} E_z(\rho_0) \\ cB_\phi(\rho_0) \end{pmatrix}. \quad (7)$$

In each case the expressions for the matrix elements may be deduced by comparison with $\hat{M}$ in Eq. (2).

For the general case where $m \neq 0$ and $\beta \neq 0$ there is no decoupling of the fields which results in hybrid modes containing all six field components. These modes may be envisaged as *skew* rays in the ray picture that spiral about the axis as they propagate along the length of the waveguide mixing the TE and TM components.[25,26]

B. Cavity design

To produce a cavity to support TPPs at a certain frequency it is necessary to provide a Bragg reflector with a stop band at that frequency. For optimum reflectivity, the reflected waves from all the dielectric interfaces of the Bragg reflector should be in phase, which in a planar Bragg reflector is achieved

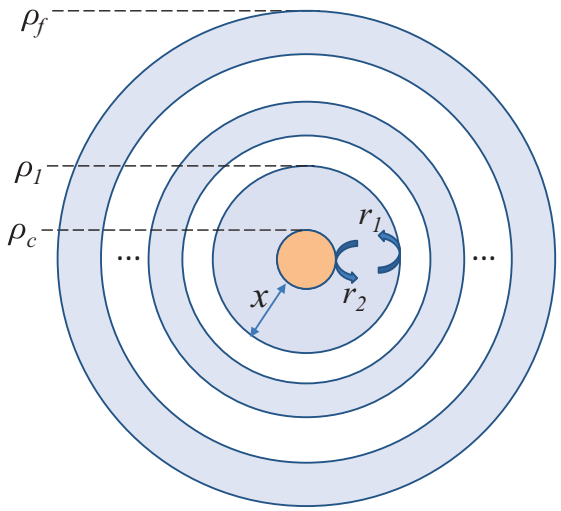

FIG. 2. (Color online) The round trip phase difference in a cavity adjacent to a metal core is given by the phase change on reflection from the Bragg reflector (r_1), the phase change on reflection from the metal (r_2), and twice the phase change of a wave traveling across the dielectric layer marked x. The dots represent repeated layers of the Bragg reflector. Key radii are marked: ρ_c is the core radius, ρ_1 is the outer radius of the first dielectric layer, and ρ_f is the outer radius of the final layer of the structure.

when each type of layer has a specific thickness, which is independent of its position within the structure. However, in a cylindrical Bragg reflector the optimal thickness of each layer varies with its radial position. A numerical method for calculating the layer thicknesses for the optimum cylindrical Bragg reflector is given in Ref. 27 but here for simplicity we use constant, quarter wavelength thicknesses which are generally accepted to provide effective reflection of cylindrical waves in most circumstances.[28] Also, for a TPP to exist there should be a phase change equal to an integer multiple of 2π or zero in a "round trip" of the radiation in the cavity formed by the metal and the Bragg reflector, as illustrated in Fig. 2 for a metal core and in Fig. 3 for a metal cladding.

There are three components to the round trip phase difference: the phase changes on reflection from the metal and the Bragg reflector and the phase change of the wave on traveling from the inner to the outer radius of the dielectric layer and back again. We note that for cylindrical waves the initial and final radii are significant for calculating the phase change resulting from propagation and not just the layer thickness as is the case for plane waves.

A method for calculating the reflection coefficient from the inside of a cylindrical Bragg reflector, the reflection marked r_1 in Fig. 2, is presented in Ref. 28 for the case of TE- and TM-polarized waves ($\beta = 0$). The same approach can be used to obtain the reflection coefficients marked r_2 in Fig. 2 and r_3 and r_4 in Fig. 3. For r_1 in the TM case we have

$$r_1^{TM} = \frac{in_f C_{mf}^{(1)} A_m^{(1)TM} - T_{21}^{TM} - in_1 C_{m1}^{(1)} T_{22}^{TM}}{T_{21}^{TM} + in_1 C_{m1}^{(2)} T_{22}^{TM} - in_f C_{mf}^{(1)} A_m^{(2)TM}}, \tag{8}$$

where

$$A_m^{(j)TM} = T_{11}^{TM} + in_1 C_{m1}^{(j)} T_{12}^{TM},$$

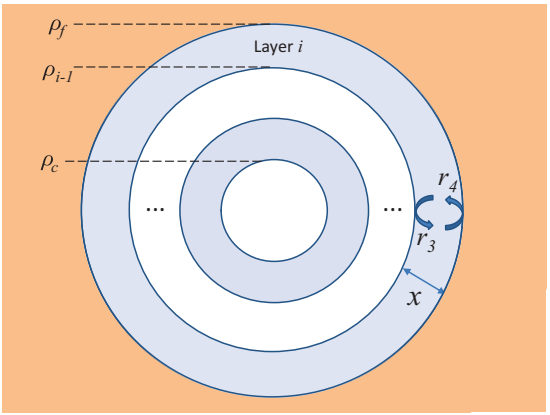

FIG. 3. (Color online) The round trip phase difference in a cavity adjacent to an essentially infinite metal cladding is given by the phase change on reflection from the Bragg reflector (r_3), the phase change on reflection from the metal (r_4), and twice the phase change of a wave traveling across the dielectric layer marked x. The dots represent repeating layers of the Bragg reflector.

n_1 is the refractive index of the dielectric layer adjacent to the metal core, n_f the refractive index outside the structure, the T_{ij} are the elements of the transfer matrix T relating the field at ρ_f to that at ρ_1, and

$$C_{mi}^{(1,2)} = \frac{H_m^{(1,2)'}(k_i\rho)}{H_m^{(1,2)}(k_i\rho)},$$

where the $H_m^{(1,2)}(k_i\rho)$ are Hankel functions and i denotes the layer.

For the TE mode:

$$r_1^{TE} = \frac{-\frac{i}{n_f} C_{mf}^{(1)} A_m^{(1)TE} - T_{21}^{TE} + \frac{i}{n_1} C_{m1}^{(1)} T_{22}^{TE}}{T_{21}^{TE} - \frac{i}{n_1} C_{m1}^{(2)} T_{22}^{TE} + \frac{i}{n_f} C_{mf}^{(1)} A_m^{(2)TE}} \tag{9}$$

where

$$A_m^{(j)TE} = T_{11}^{TE} - \frac{i}{n_1} C_{m1}^{(j)} T_{12}^{TE}.$$

The reflection coefficient marked r_2 in Fig. 2, for light incident on a cylindrical metal core, with refractive index $n_M = i\alpha$, from a dielectric material with refractive index n_1 is for the TM mode given by

$$r_2^{TM} = -\left[\frac{1 - \left(n_1 C_{m1}^{(2)}/\alpha d_m\right)}{1 - \left(n_1 C_{m1}^{(1)}/\alpha d_m\right)}\right], \tag{10}$$

where $d_m = I_m'(\alpha k_0\rho_c)/I_m(\alpha k_0\rho_c)$ in terms of modified Hankel functions. For the TE polarization

$$r_2^{TE} = -\left[\frac{1 + \left(\alpha C_{m1}^{(2)}/n_1 d_m\right)}{1 + \left(\alpha C_{m1}^{(1)}/n_1 d_m\right)}\right]. \tag{11}$$

In the case of a metal-clad Bragg reflector, we must consider the reflection coefficients denoted by r_3 and r_4 in Fig. 3. At the Bragg reflector r_3^{TM} is

$$r_3^{TM} = \frac{in_f C_{mf}^{(2)} P - Q}{Q - in_f C_{mf}^{(1)} P}, \tag{12}$$

where $P = T_{11}^{TM} J_m(k_c\rho_c) + T_{12}^{TM} i n_c J_m^{'}(k_c\rho_c)$, $Q = T_{21}^{TM} J_m(k_c\rho_c) + T_{22}^{TM} i n_c J_m^{'}(k_c\rho_c)$ and the transfer matrix elements have been calculated to describe the field as it evolves from core to exterior. The corresponding reflection coefficient for the TE polarization is

$$r_3^{TE} = -\frac{q + \left(iC_{mf}^{(2)} p\right)/n_f}{q + \left(iC_{mf}^{(1)} p\right)/n_f}, \tag{13}$$

where $p = T_{11}^{TE} J_m(k_c\rho_c) - T_{12}^{TE} i J_m^{'}(k_c\rho_c)/n_f$ and $q = T_{21}^{TE} J_m(k_c\rho_c) - T_{22}^{TE} i J_m^{'}(k_c\rho_c)/n_f$.

At the metal cladding, the reflection coefficients are:

$$r_4^{TM} = -\left[\frac{1 - \left(n_i C_{mi}^{(1)}/\alpha g_m\right)}{1 - \left(n_i C_{mi}^{(2)}/\alpha g_m\right)}\right], \tag{14}$$

$$r_4^{TE} = -\left[\frac{1 - \left(\alpha C_{mi}^{(1)}/n_i g_m\right)}{1 - \left(\alpha C_{mi}^{(2)}/n_i g_m\right)}\right], \tag{15}$$

where $= g_m = K_m^{'}(\alpha k_0\rho_f)/K_m(\alpha k_0\rho_f)$.

Finally, we point out that reflection spectra can sometimes be used as a relatively quick and easy method of seeking out the modes of cavities. For example, Fig. 4 shows the phase spectrum of the TM, $m = 0$ reflection coefficient for an incoming cylindrical wave incident on a cavity with a TiO_2 core surrounded by a cylindrical Bragg reflector comprising nine pairs of SiO_2/TiO_2 layers. The sharp feature is the signature of a TM cavity mode at 0.9234 eV. Similar behavior has been reported in planar Bragg reflector structures, e.g., Ref. 29. It should be noted that the magnitude of the reflection coefficient is unity at all frequencies when all the materials in the structure are lossless, as is apparent from Eq. (12) and the geometry of the system and the incident wave.

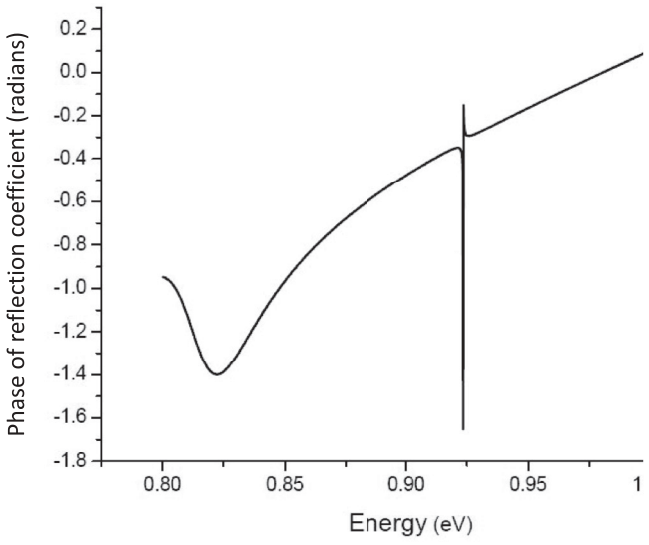

FIG. 4. The phase of the TM, $m = 0$ reflection coefficient of an incoming cylindrical wave incident on the outside of an optical cavity formed from a 150 nm TiO_2 core and a Bragg reflector with nine pairs of SiO_2/TiO_2 layers of thicknesses 211 nm and 131 nm and refractive indexes 1.47 and 2.37, respectively. There is a distinct feature in the phase variation at 0.9234 eV.

III. RESULTS

A. Metal core

To illustrate the properties of Tamm plasmon polaritons (TPPs) in cylindrical structures, we look at examples of systems that can support the excitations at energies close to 1 eV. As the first example we consider a cylindrical Bragg reflector with a metallic core as illustrated in Fig. 2. The core is chosen to be gold, which we take to have a plasma frequency $\omega_p = 8.9$ eV, and for simplicity we neglect the loss term in its dielectric response. The core has a radius of 30 nm and the layer adjacent to it is TiO_2, which is surrounded by eight pairs of SiO_2/TiO_2 layers forming a reflector. The optical thickness of each layer in the reflector is chosen to be a quarter wavelength to create a photonic stop band centered close to 1 eV (free space wavelength of 1240 nm), giving layer thicknesses of 211 nm and 131 nm for the SiO_2 (refractive index $n = 1.47$) and TiO_2 (refractive index $n = 2.37$), respectively.

It remains to calculate the required thickness of the TiO_2 layer adjacent to the metal for the structure to support a Tamm plasmon-polariton mode close to 1 eV, and that can be done by recognizing that the total phase change for a round trip in the TiO_2 layer surrounding the metal should be an integer multiple of 2π or zero. In the case of a TE mode, the phase change on reflection from the Bragg reflector may be calculated from Eq. (9) and for reflection from the metal core using Eq. (11). The phase change associated with the propagation across the TiO_2 layer is obtained by considering the ratio of the appropriate Hankel functions. By following that procedure we are able to show that there are TE and TM modes with frequency 1 eV at $\beta = 0$ with the instantaneous fields illustrated in Fig. 5. Both structures consist of a 30 nm metal core surrounded by a TiO_2 layer and then eight pairs of SiO_2/TiO_2 Bragg reflector layers. The only difference is in the

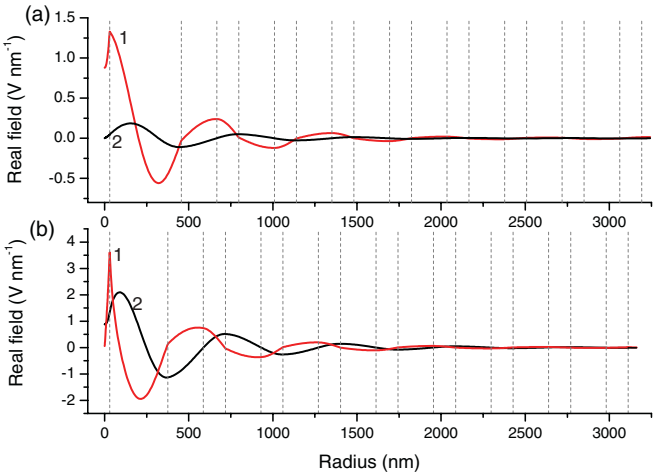

FIG. 5. (Color online) (a) cB_z (curve 1, red) and E_ϕ (2, black) field components for the TE mode with $\beta = 0$ and frequency 1 eV in a structure with a metal core of radius 30 nm and a TiO_2 layer adjacent to the metal of thickness of 426 nm. (b) cB_ϕ (curve 1, red) and E_z (2, black) field components for the TM mode with $\beta = 0$ and frequency 1 eV in an identical structure except that the TiO_2 layer adjacent to the metal has a thickness of 346 nm. The vertical dashed lines indicate the radii of the metal-dielectric and dielectric-dielectric interfaces.

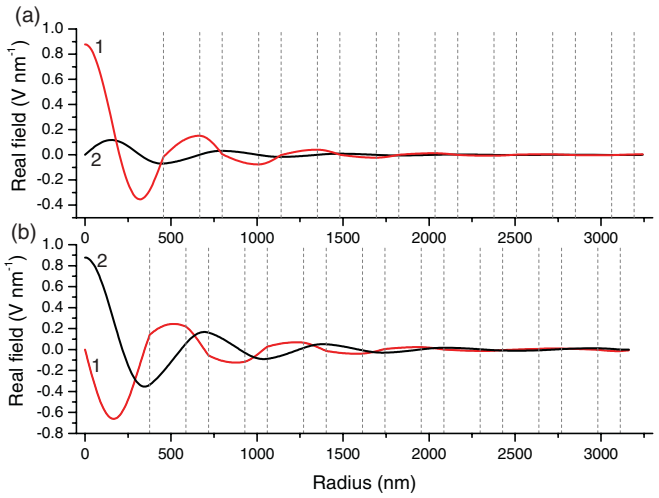

FIG. 6. (Color online) (a) cB_z (curve 1, red) and E_ϕ (2, black) field components for the TE mode with $\beta = 0$ and frequency 0.9976 eV in a multilayer structure with a TiO_2 core of radius 456 nm surrounded by eight pairs of SiO_2/TiO_2 layers. (b) cB_ϕ (1, red) and E_z (2, black) field components for the TM mode with $\beta = 0$ and frequency 0.9200 eV in an identical structure except that the TiO_2 core radius is 376 nm. The vertical dashed lines indicate the radii of the dielectric interfaces.

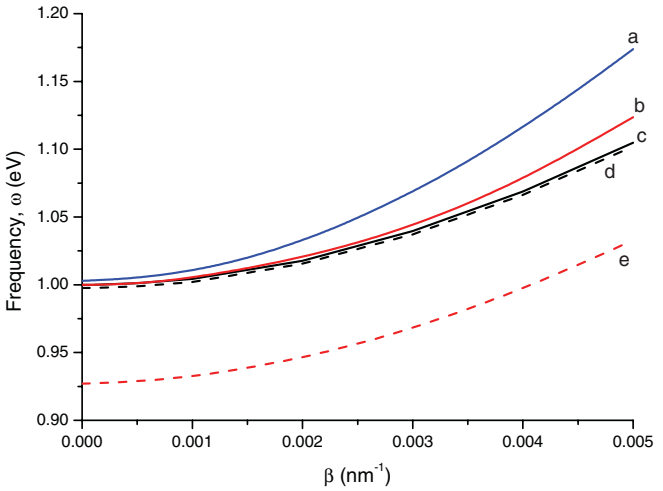

FIG. 7. (Color online) Dispersion curves for: a hybrid mode with $m = 1$ in a cavity with a 30 nm radius metal core surrounded by an SiO_2 cavity layer of thickness 483 nm and eight pairs of TiO_2/SiO_2 layers [(a), solid blue line]; TM [(b), solid red)] and TE [(c), solid black] modes for the structures required to give a mode frequency at $\beta = 0$ of 1 eV; TE [(d), dashed black] and TM [(e), dashed red] modes for an identical structure except that the metal core has been replaced by TiO_2.

thickness of the TiO_2 layer adjacent to the metal; in the case of the TE mode the thickness is 426 nm and for the TM mode, 346 nm. The vertical dashed lines indicate the dielectric boundaries and it is clear that the field components have the characteristic decay of a TPP state in the metal and the Bragg reflector.

In a planar structure, light in TiO_2 normally incident on an infinite SiO_2/TiO_2 Bragg reflector at the center frequency of its first stop band would have an (electric field) reflection coefficient equal to unity and hence the electric field would have an antinode at the first TiO_2-SiO_2 interface. A similar behavior is to be seen in the cylindrical structures considered here where for the TE mode E_ϕ has an antinode (and hence according to Maxwell's $\nabla \times \mathbf{E}$ equation, B_z has a node) and for the TM mode E_z an antinode (and B_ϕ a node).

Figure 6 shows the instantaneous field components for the TE and TM modes that exist for $\beta = 0$ for the same structures as considered in connection with Fig. 5 but without the metal core. In each case the 30 nm metal core has been replaced by TiO_2. Comparing Fig. 6 to Fig. 5 it is clear that the removal of the metal makes very little difference to the field components of the TE mode but the changes at the center of the structure are substantial for the TM mode.

For the structures with the metallic core, increasing the propagation constant β from zero and finding the corresponding mode frequencies gives the dispersion curves shown in Fig. 7 exhibiting TE-TM splitting at nonzero β. Also shown are the curves for the same structures but with the metal core removed and replaced by TiO_2, and the dispersion curve for a hybrid mode with $m = 1$, $\beta = 0$ in a structure consisting of a 30 nm metal core surrounded by a SiO_2 cavity layer of thickness 483 nm and eight pairs of TiO_2/SiO_2 layers. The dispersion curves for the TE modes with and without the metallic core are very similar but there is a significant frequency difference in the TM curves (80 meV at $\beta = 0$) reflecting the substantial difference in the fields between Figs. 5 and 6 for that mode.

As a result of the transverse confinement afforded by the cylindrical Bragg reflector, all the dispersion curves are very different from those of a conventional optical fiber, which all lie between the light lines for the fiber core and cladding. In the structures considered here, the mode frequencies are nonzero at zero propagation constant β and have an essentially parabolic dependence on β, with effective masses of $1.4 \times 10^{-6} m_e$ for the TE mode, $1.2 \times 10^{-6} m_e$ for the TM mode, and $0.83 \times 10^{-6} m_e$ for the $m = 1$ mode. The group velocity may also be calculated; for example at $\beta = 1 \times 10^{-6}$ nm^{-1} the group velocity is 0.8×10^5 ms^{-1} for the TE mode, 1.0×10^5 ms^{-1} for the TM mode, and 1.4×10^5 ms^{-1} for the $m = 1$ hybrid mode, all of which are orders of magnitude lower than the speed of light in vacuum or in TiO_2.

B. Metal cladding

Next we consider a structure, such as that illustrated in Fig. 3, which is a cylindrical Bragg reflector surrounded by a cavity layer with an infinite metal cladding. Figure 8 shows the instantaneous, real E_z and cB_ϕ field components for a TM mode with $m = 0$, $\beta = 0$ and frequency 1 eV, for a structure with a TiO_2 core of radius 150 nm surrounded by 14 pairs of TiO_2/SiO_2 layers. As previously, the thicknesses of the SiO_2 and TiO_2 layers are 211 nm and 131 nm, respectively. Within the metal cladding there is a SiO_2 cavity layer of thickness 400 nm surrounding the Bragg reflector structure. Again we take the plasma frequency of the metal to be 8.9 eV and neglect the loss term in its dielectric response. The radius of the core was chosen so that it would not support a mode at the center of the structure. The thickness of the cavity layer was chosen to support a round trip phase change of 2π. The fields can be seen to decay both into the metal (to the right of the final

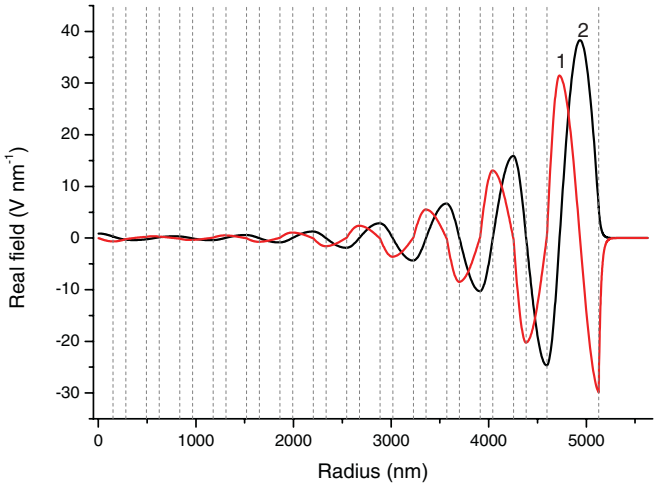

FIG. 8. (Color online) cB_ϕ (curve 1, red) and E_z (2, black) field components of a TM mode of frequency 1.0 eV in a multilayer structure with a 150 nm TiO_2 core, 14 pairs of TiO_2/ SiO_2 layers and a SiO_2 cavity layer of thickness 400 nm all surrounded by an infinite metal cladding. The vertical dashed lines indicate the radii of the metal-dielectric and dielectric-dielectric interfaces.

boundary line) and into the Bragg reflector (to the left of the final boundary line).

As another example, Fig. 9 shows the real cB_z and E_ϕ fields for the TE, $m = 0$, $\beta = 0$ mode at frequency 1 eV in a multilayer cylindrical structure with a TiO_2 core of radius 150 nm surrounded by 14 pairs of SiO_2/TiO_2 layers and a TiO_2 cavity layer of thickness 130 nm all enclosed in a lossless metal with plasma frequency 8.9 eV. It can be seen that the field is greatest inside the cavity layer adjacent to the metal and decays very rapidly into the metal and more slowly into the Bragg reflector structure.

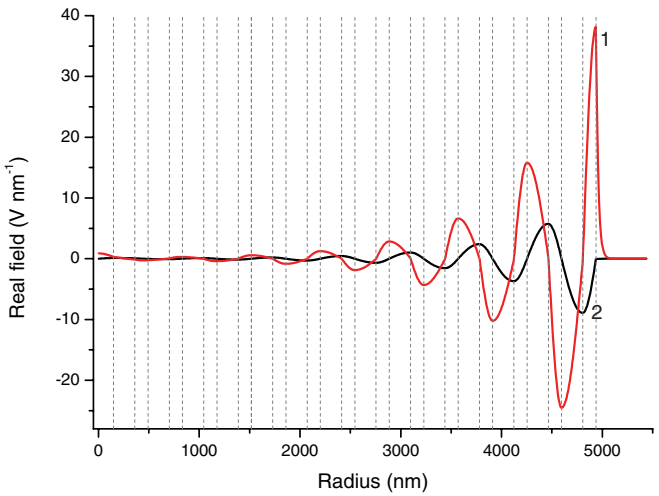

FIG. 9. (Color online) cB_z (curve 1, red) and E_ϕ (2, black) field components of a TE mode with frequency 1 eV and $\beta = 0$ in a structure with a TiO_2 core of radius 150 nm surrounded by 14 pairs of SiO_2/TiO_2 layers and a TiO_2 cavity layer with a thickness of 130 nm adjacent to the metal cladding. The vertical dashed lines indicate the radii of the metal-dielectric and dielectric-dielectric interfaces.

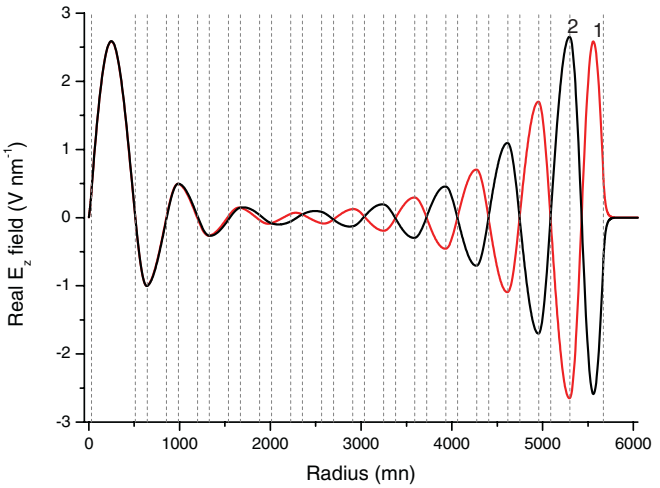

FIG. 10. (Color online) E_z field components for two split modes, one with frequency 1.00589 eV (curve 1, red) and the other with frequency 1.00406 eV (2, black). Both were calculated for $m = 1$, $\beta = 0$ in a structure consisting of: a metal core of radius 30 nm; a SiO_2 cavity layer adjacent to the core of thickness 483 nm; 14 pairs of layers alternating TiO_2/SiO_2 with respective thickness 131 nm/211 nm; a final TiO_2 cavity layer of thickness 370 nm adjacent to the semi-infinite metal cladding. The vertical dashed lines indicate the radii of the metal-dielectric and dielectric-dielectric interfaces.

In both these examples the frequency at the center of the photonic band gap of the Bragg reflector was chosen to be 1 eV and the structure was designed accordingly. Note that the order of the layers in the Bragg reflector to support a TE mode is the opposite of that required to support a TM mode.

C. Metal core and cladding

Figure 10 shows the instantaneous, real, E_z field components for the split modes of a coupled multilayered system with $m = 1$ and $\beta = 0$. The structure has a 30 nm metal core and semi-infinite metal cladding outside. There is a SiO_2 cavity layer adjacent to the metal core with a thickness of 483 nm and a TiO_2 cavity layer adjacent to the metal cladding with a thickness of 370 nm. The interim Bragg reflector structure has 14 pairs of alternating TiO_2/SiO_2 layers of thickness 131 nm/211 nm respectively. Close to the core, this structure is the same as that considered for supporting the $m = 1$, $\beta = 0$ mode for the case with metal in the core only. The fields of the two modes in Fig. 10 can be seen to follow essentially the same pattern close to the core but progressively become out of phase in the Bragg reflector layers and are in antiphase at the outer edge. As such they represent symmetric and antisymmetric modes and are characterized by dispersion curves and group velocities very similar to those of the $m = 1$ mode in Fig. 6. The frequency splitting between the modes is just 1.83 meV or 0.44 THz and since that depends on the overlap of the electromagnetic fields of the inner and outer modes in the Bragg reflector layers when they are considered separately, it can be varied by changing the number of layers in the Bragg reflector.

IV. DISCUSSION

It has been shown that TPPs in cylindrical structures have low group velocities, as is the case for planar TPPs. Slow light has a compressed spatial pulse length which may give a longer interaction time and an enhancement of the light-matter interaction compared with light traveling at more conventional speeds.[30] Slow light has also been proposed as a useful tool in information processing;[31] some logic elements require a time delay in processing and current attempts to achieve this in photonics make use of long optical fibers, which means that the scale of the components is necessarily large. Another area of potential applications is terahertz technology. The terahertz frequency splitting of the modes of cylindrical structures with both metallic core and cladding is analogous to that which can occur with suitably designed coupled planar cavities in semiconductor structures (see for example Ref. 32) and makes possible the production of radiation with a terahertz beat frequency. However, the waveguide geometry has the great advantage of facilitating flexible spatial control in the delivery of that radiation. More generally, the cylindrical waveguide structure provides opportunities to manipulate the azimuthal properties of TPPs and of light emerging from the end of guide by the use of longitudinal metallic stripes and helices on the outer cylindrical surface.

The materials in the Bragg reflector structures considered, TiO_2 and SiO_2 were chosen due to their large refractive index contrast while having a relatively mechanically robust and chemically inert nature. Both materials have widespread technological uses, and SiO_2 is routinely used in the fabrication of optical fibers. Coating a fiber with metal by evaporation would be straightforward but there are substantial technical challenges in producing the other features of the structures we have considered. It may be possible to produce multilayer dielectric structures by sputtering additional layers on an initial core dielectric fiber or metal wire, but the precision required in the thickness of each layer needs to be of the order of a few nanometers and would prove challenging using current technology. However, despite the obvious difficulties in fabricating cylindrical multilayer structures, the current intense interest in optics and plasmonics on the nanoscale can be expected to encourage the necessary innovations.

Optical loss through the cylindrical Bragg reflector structures is normally small and can safely be neglected. Also, all the materials have been modeled as lossless for calculational simplicity. The electronic band gaps of both SiO_2 and TiO_2 are large enough to avoid significant absorption at the photon energies of interest. The precise values of the refractive indices depend on the fabrication process as well as wavelength and therefore the values used here are merely representative. Loss in the metal could be included by having a complex relative permittivity. Including losses in the calculations would then involve finding zeros in the determinant of the matrix in Eq. (5) in the complex plane. However, the waveguide attenuation can also be estimated using the fields obtained for the lossless case by treating the imaginary part of the susceptibility of the metal as a perturbation. Using that approach, we find quality factors Q that are generally greater than 10^3 for the cylindrical cavities considered here. The inverse attenuation constant follows as $2Qv_g/\omega$ giving values, depending on the group velocity v_g of up to several hundred micrometers, and similar to conventional surface plasmon technology.[33] In fact, in practice TPP structures can be expected to have significantly lower attenuation due to the much smaller proportion of the field energy that resides in the metal as a result of the different confinement mechanism on the dielectric side of the interface.

V. CONCLUSIONS

It has been shown theoretically that cylindrical Bragg reflector structures are capable of supporting Tamm plasmon polaritons by having a metal core, metal cladding around the outside of the structure, or metal in both of these locations. The cylindrical TPPs can exist in both the TE and TM polarizations for the special cases $m = 0$ or $\beta = 0$ and can also be formed from hybrid cylindrical modes when $m \neq 0$ and $\beta \neq 0$. In the cases considered, the excitations have low effective masses and group velocities that are smaller by a factor of 10^3 than light, making the phenomenon attractive as the basis of optical delay lines. When there is metal both at the core and around the outside of the Bragg reflector, structures can be designed in which pairs of modes have a frequency difference in the terahertz regime suggesting that the structures could have applications in related technologies.

ACKNOWLEDGMENTS

The authors are grateful for very useful discussions with A. V. Kavokin and acknowledge funding through an EPSRC PhD studentship, the EU FP7 POLALAS (230811) and CLERMONT4 (235114) projects, and the Russian Foundation for Basic Research.

*r.a.abram@durham.ac.uk

[1] M. Kaliteevski, I. Iorsh, S. Brand, R. A. Abram, J. M. Chamberlain, A. V. Kavokin, and I. A. Shelykh, Phys. Rev. B **76**, 165415 (2007).

[2] A. V. Kavokin, I. A. Shelykh, and G. Malpuech, Phys. Rev. B **72**, 233102 (2005).

[3] M. E. Sasin, R. P. Seisyan, M. A. Kaliteevski, S. Brand, R. A. Abram, J. M. Chamberlain, A. Y. Egorov, A. P. Vasil'ev, V. S. Mikhrin, and A. V. Kavokin, Appl. Phys. Lett. **92**, 251112 (2008).

[4] S. Brand, M. A. Kaliteevski, and R. A. Abram, Phys. Rev. B **79**, 085416 (2009).

[5] S. Brand, R. A. Abram, and M. A. Kaliteevski, J. Phys. D **43**, 145104 (2010).

[6] C. Symonds, A. Lemaître, E. Homeyer, J. C. Plenet, and J. Bellessa, Appl. Phys. Lett. **95**, 151114 (2009).

[7] C. Grossmann, C. Coulson, G. Christmann, I. Farrer, H. E. Beere, D. J. Ritchie, and J. J. Baumberg, Appl. Phys. Lett. **98**, 231105 (2011).

[8]C. Symonds, A. Lemaître, P. Senellart, M. H. Jomaa, S. A. Guebrou, E. Homeyer, G. Brucoli, and J. Bellessa, Appl. Phys. Lett. **100**, 121122 (2012).
[9]O. Gazzano, S. M. de Vasconcellos, K. Gauthron, C. Symonds, J. Bloch, P. Voisin, J. Bellessa, A. Lemaître, and P. Senellart, Phys. Rev. Lett. **107**, 247402 (2011).
[10]M. Kaliteevski, S. Brand, R. A. Abram, I. Iorsh, A. V. Kavokin, and I. A. Shelykh, Appl. Phys. Lett. **95**, 251108 (2009).
[11]T. C. H. Liew, A. V. Kavokin, T. Ostatnický, M. Kaliteevski, I. A. Shelykh, and R. A. Abram, Phys. Rev. B **82**, 033302 (2010).
[12]R. Brückner, M. Sudzius, S. I. Hintischich, H. Fröb, V. G. Lyssenko, M. A. Kaliteevski, I. Iorsh, R. A. Abram, A. V. Kavokin, and K. Leo, Appl. Phys. Lett. **100**, 062101 (2012).
[13]G. Du, H. Jiang, Z. Wang, Y. Yang, Z. Wang, H. Lin, and H. Chen, J. Opt. Soc. Am. B **27**, 1757 (2010).
[14]W. L. Zhang and S. F. Yu, Opt. Commun. **283**, 2622 (2010).
[15]C. Xue, H. Jiang, and H. Chen, Opt. Exp. **18**, 7479 (2010).
[16]T. Goto, A. V. Baryshev, M. Inoue, A. V. Dorofeenko, A. M. Merzlikin, A. P. Vinogradov, A. A. Lisyansky, and A. B. Granovsky, Phys. Rev. B **79**, 125103 (2009).
[17]L. Dong, H. T. Jiang, H. Chen, and Y. Shi, J. Appl. Phys. **107**, 093101 (2010).
[18]C. A. Pfeiffer, E. N. Economou, and K. L. Ngai, Phys. Rev. B **10**, 3038 (1974).
[19]U. Schröter and A. Dereux, Phys. Rev. B **64**, 125420 (2001).
[20]S. J. Al-Bader and M. Imtaar, J. Opt. Soc. Am. B **10**, 83 (1993).
[21]B. Prade and J. Y. Vinet, J. Lightwave Tech. **12**, 6 (1994).
[22]B. Sun, Y. Gu, X. Hu, and Q. Gong, Chin. Phys. Lett. **28**, 057303 (2011).
[23]D. Chen, Appl. Opt. **49**, 6868 (2010).
[24]W. C. Chew, *Waves and Fields in Inhomogeneous Media* (Wiley-IEEE Press, New York, 1995).
[25]A. W. Snyder and J. D. Love, *Optical Waveguide Theory*, 1st ed. (Chapman and Hall, London, 1983).
[26]J. D. Jackson, *Classical Electrodynamics*, 3rd ed. (Wiley, New York, 1999).
[27]M. A. Kaliteevski, R. A. Abram, V. V. Nikolaev, and G. S. Sokolovski, J. Mod. Opt. **46**, 875 (1999).
[28]M. A. Kaliteevski, R. A. Abram, and V. V. Nikolaev, J. Mod. Opt. **47**, 677 (2000).
[29]R. L. Nelson and J. W. Haus, Appl. Phys. Lett. **83**, 1089 (2003).
[30]P. W. Milonni, *Fast Light, Slow Light, and Left-Handed Light*, 1st ed. (Taylor & Francis, New York, 2005).
[31]M. Notomi, Rep. Prog. Phys. **73**, 096501 (2010).
[32]T. Kitada, F. Tanaka, T. Takahashi, K. Morita, and T. Isu, Appl. Phys. Lett. **95**, 111106 (2009).
[33]W. L. Barnes, A. Dereux, and T. W. Ebbesen, Nature (London) **424**, 824 (2003).